Dynamic and steady state current response to light excitation of multilayered organic photodiodes

E. S. Zaus, S. Tedde, J. Fürst, D. Henseler, and G. H. Döhler

Citation: Journal of Applied Physics **101**, 044501 (2007); doi: 10.1063/1.2433712
View online: http://dx.doi.org/10.1063/1.2433712
View Table of Contents: http://scitation.aip.org/content/aip/journal/jap/101/4?ver=pdfcov
Published by the AIP Publishing

Dynamic and steady state current response to light excitation of multilayered organic photodiodes

E. S. Zaus,[a] S. Tedde, J. Fürst, and D. Henseler
Siemens AG, CT MM 1, Günther-Scharowsky-Strasse 1, 91052 Erlangen, Germany

G. H. Döhler
Max Planck Research Group for Optics, Information and Photonics, University of Erlangen-Nürnberg, Günther-Scharowsky-Strasse 1, 91052 Erlangen, Germany

(Received 16 August 2006; accepted 29 November 2006; published online 16 February 2007)

Measurements of current transients are used to gain insight into the mechanism of charge transport and extraction of photodiodes based on bulk heterojunction blends of poly-3-hexyl-thiophene and [6,6]-phenyl C_{61} butyric acid methyl ester. It is shown that the implementation of an appropriate hole conducting layer leads to a reduction of the dark current in the reverse direction. It is observed that the dynamic response to light excitation is strongly influenced by the thickness of the hole conducting layer, the light intensity, and the applied bias. Charge accumulation at the interface is assumed to result in the characteristic shape of the transients. The shape of the switch-off transient can be understood qualitatively by an equivalent circuit diagram. © *2007 American Institute of Physics*. [DOI: 10.1063/1.2433712]

I. INTRODUCTION

In the last several years organic semiconductors have been used in a variety of electronic devices. The possibility to fabricate flexible, large area, light-weight, and low-cost devices makes them attractive. Organic light emitting diodes (LEDs),[1,2] organic thin film transistors,[3] and organic photodiodes have especially attracted much attention.

An important step towards highly efficient charge separation in photovoltaic devices was the introduction of concepts of an interpenetrating network of conjugated polymers as donor material and fullerenes,[4,5] or other molecules,[6] with larger electron affinity as acceptor material. The absorption of an incident photon in the donor material of the bulk heterojunction blend results in the formation of an exciton. The exciton is dissociated by an electron transfer to the acceptor material. Charge separation times of less than 100 fs have been reported.[7,8] Because this process is more than 1000 times faster than the radiative or nonradiative decay of photoexcitations,[4,9] the quantum efficiency of charge separation is almost 100%. These properties are very promising for the application of organic photodiodes as highly efficient solar cells[10] or very sensitive photodetectors.[11]

To achieve a fast response time and a high efficiency[12] and for the realization of an integrating active-matrix readout, photodetectors are often biased in the reverse direction. A crucial requirement for the sensitivity of those devices is a low dark current density in the operating bias voltage regime. For accurate light detection the dark current should be negligible compared to the photocurrent. An approach to reduce the dark current due to injection of charge carriers from the electrodes is the implementation of an appropriate blocking layer between the electrode and the photosensitive layer. The energy levels of the highest occupied molecular orbital (HOMO) and the lowest unoccupied molecular orbital (LUMO) of this blocking layer build an injection barrier at the electrode for one charge carrier species but do not impede the extraction of the photogenerated charge carriers of the other species. A schematic example is shown in Fig. 1.

In this paper it is shown that the dark current density can be reduced significantly by implementing an electron blocking layer at the anode. Furthermore, the dynamic response to light excitation of these devices is studied to get insight into the transport mechanism and the response time of the device which is a crucial property for many applications. The resulting current transients are discussed.

II. EXPERIMENT

The layout of the studied devices was Au/hole conductor/bulk heterojunction/Ca/Ag and Au/bulk heterojunction/Ca/Ag for comparison. The 100-nm-thick Au bottom electrode was sputtered on a glass substrate. As hole conductor, poly[9,9′-dioctylfluorene-co-bis-*N*,*N*′-(4,butylphenyl)-bis-*N*,*N*′-phenyl-1,4-phenylene-diamine] (PFB) was used, which was spin cast from solution and baked at 200 °C

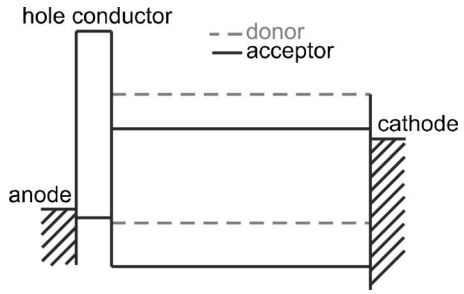

FIG. 1. Schematic energy diagram of a device with hole conductor layer between anode and donor-acceptor blend at flatband situation. The hole conductor acts as a blocking layer to prevent injection of electrons from the anode into the device due to its high LUMO level.

[a]Electronic mail: edgar.zaus.ext@siemens.com

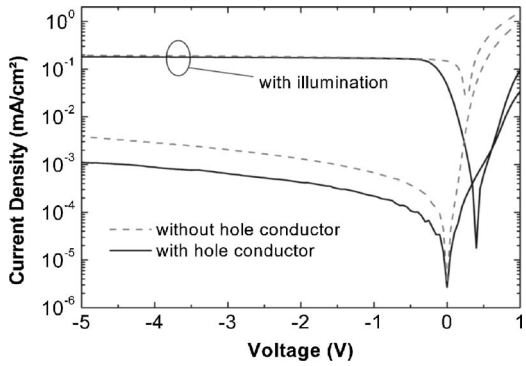

FIG. 2. Typical *I-V* characteristics of photodiodes with HC (thickness 40 nm) and without. The light intensity for the curves with illumination is 0.87 mW/cm^2.

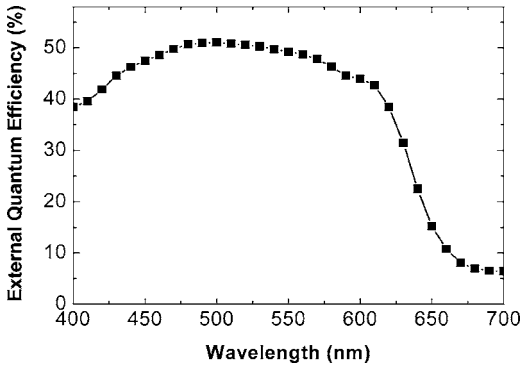

FIG. 3. Spectral plot of the external quantum efficiency (EQE) of the photodiode with HC (thickness 40 nm) for an applied bias voltage of −3 V.

for 1 h in a vacuum oven at a pressure below 5 mbars. The thickness of the hole conductor was chosen as 20 or 40 nm. A high LUMO level of 2.4 eV and a HOMO level of 5.2 eV,[13] close to the work function of Au of 5.1 eV,[14] make PFB a promising material as electron blocking layer. The bulk heterojunction consists of a blend of poly-3-hexylthiophene (P3HT) as donor material and [6,6]-phenyl C_{61} butyric acid methyl ester (PCBM) as acceptor material, which was applied by the doctor blading technique. The blending ratio of P3HT:PCBM was 1:0.75 and the layer thickness can be estimated to be 250 nm. A semitransparent top electrode, made of 3 nm Ca and 10 nm Ag, was evaporated thermally. Finally the devices were encapsulated using an epoxy resin and glass coverslip. The area of the diodes is 2×2 mm^2, defined by the overlap of the two electrodes.

The *I-V* characteristics of the diodes were measured using a Keithley 236 source measure unit. For the phototransient measurements a Lumileds Luxeon 3 Star LED was used as a light source. The maximum in the emission spectrum of the LED is located at the wavelength of about 522 nm with a spectral half-width of 35 nm. The LED was driven by a Hewlett-Packard 33120A wave form generator and an FLC F20AD voltage amplifier. 50-ms-long light pulses with a frequency of 10 Hz were applied to the photodiode. The current through the photodiode was amplified by a Femto DHPCA-100 current amplifier and displayed by a LeCroy Wavesurfer 424 oscilloscope. The response time of the setup is limited by the bandwidth of the amplifier. Taking into account the used amplification and the capacitance of the photodiode the bandwidth can be estimated to be 0.6 MHz resulting in a rise/fall time (10%–90%) of less than 1 μs. All measurements were performed at room temperature.

III. RESULTS

By implementing a hole conducting (HC) layer between the Au anode and the P3HT:PCBM blend, the dark current in the reverse direction can be significantly reduced. In Fig. 2 typical *I-V* characteristics of devices with and without HC are shown on a semilogarithmic scale. At a bias voltage of −5 V the dark current is lowered by a factor of 4. Another interesting feature of the *I-V* characteristics is the shape of the curves with illumination. Going from forward to reverse bias voltages, the current reaches a plateau value at 0 V for the diode without HC. However, in the case of the diode with interlayer a bias voltage of approximately −0.2 V is necessary to reach the plateau value (photocurrent saturation regime).

The external quantum efficiency (EQE) of a photodiode with HC is shown in Fig. 3. At the applied reverse bias voltage of −3 V the diode is driven in the photocurrent saturation regime. The EQE values are close to the transmittance values of the top electrode in the wavelength range of 450–600 nm, which reflects the high internal quantum efficiencies in that range.[15] That means that for the illumination with the LED (almost) all photons reaching the active layer contribute to the photocurrent.

To get information about the influence of the HC on the dynamic response to light excitation of the photodiode, a light pulse was applied to the photodiode and current transients were recorded for zero applied bias. The dependence on the illumination intensity is shown in Fig. 4. For higher intensities the current increases within 1 ms to a peak value and then decreases to a steady state value. (For comparison a curve of a device without HC is also displayed in Fig. 4, which shows no peak.) The time necessary to reach the steady state value decreases and the peak current density increases linearly with increasing illumination intensity, see inset of Fig. 4. (The slope of the double-logarithmic plot is

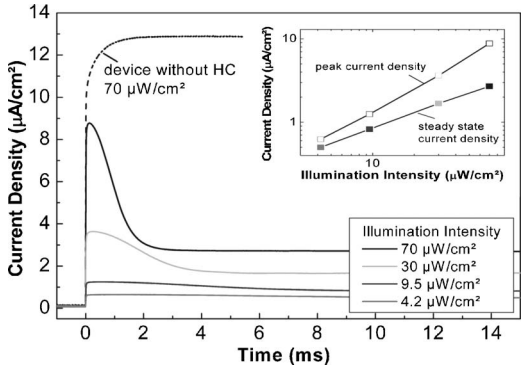

FIG. 4. Dependence of the current transients on the illumination intensity for no bias voltage applied to the diode. The inset shows the dependence of peak and steady state current density on the illumination intensity of the device with HC on a double-logarithmic scale. The slopes of the power-law fits are 0.93 for the peak current density data (nearly linear dependence) and 0.60 for the steady state current density data (sublinear dependence). The light pulse starts at 0 s and has a duration of 50 ms.

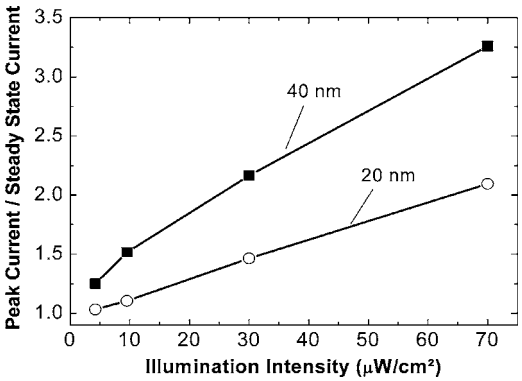

FIG. 5. Dependence of the strength of the peaks on the illumination intensity for devices with 20 and 40 nm HC thicknesses. No bias voltage applied to the diode.

almost unity. In contrast, the slope of the steady state current density is sublinear.) The ratio of peak current to steady state current is a measure for the strength of the peak. Figure 5 shows this ratio for the two thicknesses of the HC as a function of illumination intensity. It decreases with lower thickness of the HC.

The shape of the transients changes drastically if a bias voltage is applied [Fig. 6(a)]. At sufficiently high reverse bias voltage the initial peaks disappear and the shapes become similar to the shape of photodiodes without HC [Fig. 6(b)]. The time to reach the steady state value is even lower for the device with HC (1.5 ms at −3 V bias voltage) than without (2.5 ms). Additional measurements (not shown here) show good signal linearity of the steady state current if a sufficiently large reverse bias voltage is applied in contrast to the case without (inset of Fig. 4). The transition ranges from

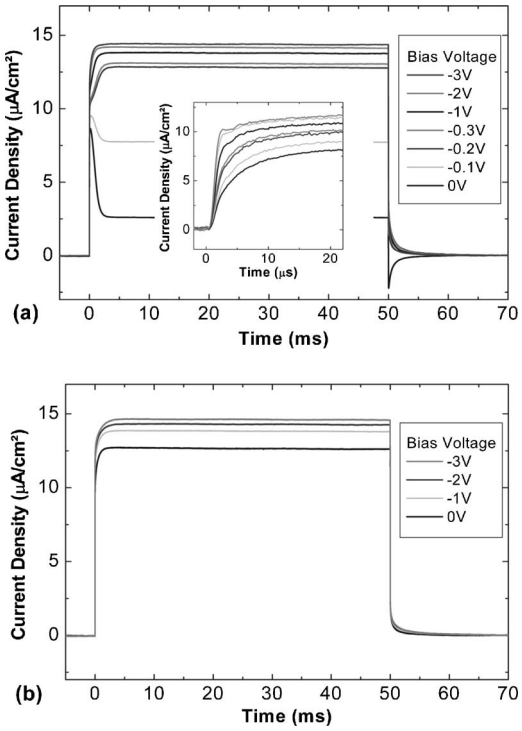

FIG. 6. Dependence of the current transients on the applied bias voltage for a device with HC (a) and without (b). The illumination intensity is 70 $\mu W/cm^2$ for both cases.

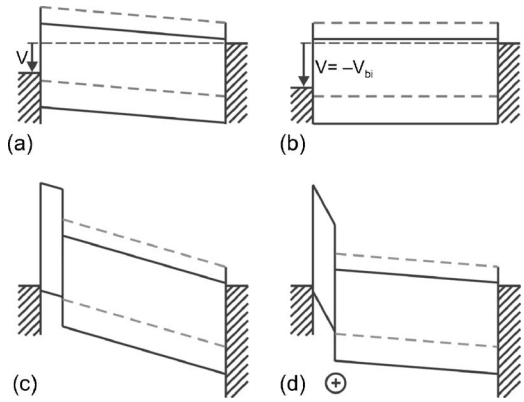

FIG. 7. Schematic picture of the HOMO and LUMO levels of a device without HC [(a) and (b)] and with HC [(c) and (d)]. In (b) the external bias voltage V compensates the built-in voltage so that the electric field within the device is zero. In (c) and (d) no external bias voltage applied. At steady state the electric field in the blend layer is reduced due to the accumulated charge at the blend-HC interface.

0 to about −0.2 V, which corresponds to the voltage value in the *I-V* characteristics at which a constant current is achieved under illumination (cf. Fig. 2). At low reverse bias voltage a negative peak can be observed when the light is switched off.

IV. DISCUSSION

In the following, a model is presented which is able to explain the observations qualitatively. As described in the Introduction, the incident photons are absorbed by the blend (thickness d_B) and electrons and holes are generated. The photocurrent is characterized by exciton dissociation probability close to unity, mobilities μ_p and μ_n, and recombination lifetimes τ_p and τ_n, respectively. In the detector without HC the electric field in the blend, F_B, is determined simply by the sum of the built-in voltage V_{bi} and the external voltage V divided by d_B. In the flatband situation [$V=-V_{\mathrm{bi}}$; Fig. 7(b)] F_B is zero. Therefore, there is no photocurrent and the photogenerated holes and electrons recombine within a diffusion length from the point where they were created. At finite fields the drift length is $\Lambda_{\mathrm{dr},p}=\mu_p\tau_p F_B$ or $\Lambda_{\mathrm{dr},n}=\mu_n\tau_n F_B$, respectively. At sufficiently high fields, finally, the drift length exceeds the layer thickness d_B, i.e., $\mu_p\tau_p F_B > d_B$ and/or $\mu_n\tau_n F_B > d_B$. This saturation regime occurs once this condition is fulfilled for the carriers with the larger $\mu\tau$ product, in our case for the holes. This reads

$$\mu_p\tau_p F_{\mathrm{sat}} = d_B. \tag{1}$$

In this regime (nearly) all the photogenerated holes reach the anode. This implies that in the stationary state also all the electrons ultimately reach the cathode because of the requirement of charge conservation. The ideal current density under an optical illumination intensity I_{opt}, with each incident photon of energy $h\nu$ creating an electron-hole pair, then becomes

$$j_{\mathrm{sat}} = qI_{\mathrm{opt}}/h\nu. \tag{2}$$

For $F_B \ll F_{\mathrm{sat}}$ the stationary current is reduced by the ratio of the actual *Schubweg* $\mu_p\tau_p F_B$ to the blend layer thickness d_B:

$$j = \frac{\tau_p\mu_p F_B}{d_B} j_{\mathrm{sat}} = \frac{F_B}{F_{\mathrm{sat}}} j_{\mathrm{sat}}. \tag{3}$$

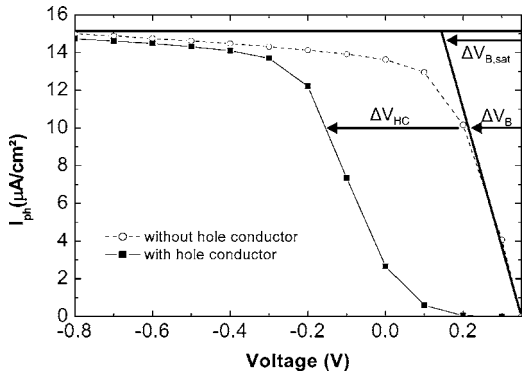

FIG. 8. Steady state photocurrent density of devices with and without HC under illumination intensity of 70 μW/cm^2. The photocurrent was calculated from the current densities with and without illumination: $I_{\mathrm{ph}}=I_{\mathrm{illumination}}-I_{\mathrm{dark}}$. The distribution of the voltage drops over the two layers ΔV_{HC} and ΔV_B is shown for a defined photocurrent (as an example drawn in for $I_{\mathrm{ph}}=10$ μA/cm^2).

A phenomenological interpolation between the two regimes yields

$$j=\frac{F_B}{\sqrt{F_{\mathrm{sat}}^2+F_B^2}}j_{\mathrm{sat}}. \tag{4}$$

The hole density at the interface to the HC is reduced by the same factor, i.e.,

$$p=\frac{F_B}{\sqrt{F_{\mathrm{sat}}^2+F_B^2}}p_{\mathrm{sat}}, \tag{5}$$

with

$$p_{\mathrm{sat}}=\frac{j_{\mathrm{sat}}}{q\mu_p F_{\mathrm{sat}}}=\frac{j_{\mathrm{sat}}\tau_p}{qd_B}. \tag{6}$$

From the stationary photocurrent versus voltage curves for the detector without HC (dashed line in Fig. 2) we see that in this case the saturation current is reached at a voltage of about $V_{B,\mathrm{sat}}=0.1$ V. We also see that the photocurrent is zero at about $V_{B,\mathrm{oc}}=0.3$ V. This "open-circuit voltage" corresponds very closely to the flatband voltage [$V=-V_{\mathrm{bi}}$; Fig. 7(b)], as the dark current at this voltage is by more than an order of magnitude lower than the saturation photocurrent. Thus, the saturation field $F_{B,\mathrm{sat}}=\Delta V_{B,\mathrm{sat}}/d_B=(V_{B,\mathrm{oc}}-V_{B,\mathrm{sat}})/d_B$ turns out to be $F_{B,\mathrm{sat}}=8\times10^3$ V/cm. In order to be able to make a quantitative analysis of both stationary and pulsed measurements the corresponding situation is also shown (now on a linear scale) for an illumination intensity of 70 μW/cm^2 as used in the pulsed measurements displayed in Fig. 8. Here, however, the dark current at $V_{B,\mathrm{oc}}$ is no longer negligible. Therefore, the photocurrent $I_{\mathrm{ph}}=I_{\mathrm{illumination}}-I_{\mathrm{dark}}$ is depicted. From a linear extrapolation of the photocurrent density to the saturation photocurrent density of about 15 μA/cm^2 we obtain $\Delta V_{B,\mathrm{sat}}=0.21$ V and, with $d_B=250$ nm, $F_{B,\mathrm{sat}}=8.4\times10^3$ V/cm. The lifetime $\tau=d_B^2/(\mu\Delta V_{B,\mathrm{sat}})$ of the charge carriers of the P3HT:PCBM blend can be estimated as 10 μs assuming a mobility μ of 3×10^{-4} cm^2/V s.[16]

In the detector with HC the generation and recombination of electron-hole pairs and their transport within the blend at a given field F_B are expected to be the same as observed in the detector without HC (as long as the electrons are not propagating towards the Au anode, where they would encounter the barrier in the LUMO band. The latter situation occurs only under a forward bias exceeding the flatband voltage, which is not considered here). In Fig. 7(c) the zero voltage band diagram is shown schematically for the dark case. Assuming similar dielectric constants for the blend and the HC together with no or negligible offset between the HOMO levels in the HC [5.2 eV (Ref. 13)] and the P3HT [5.2 eV (Ref. 17)], the built-in field is expected to be $F_{B,d}=F_{\mathrm{HCL},d}=V_{\mathrm{bi}}/(d_B+d_{\mathrm{HCL}})$.

Under illumination the field distribution becomes determined by the interplay between current continuity condition and field changes due to the buildup of space or interface charges. The stationary state situation is depicted schematically, again for zero applied voltage, in Fig. 7(d). As photoelectrons are neither being generated in the HC nor arriving at the interface, all the holes arriving at the interface will ultimately arrive at the anode as there are no partners for recombination. Thus, the current continuity condition requires that at the interface and within the whole HC the relation

$$j_p=q\mu_{p,\mathrm{HC}}p_{\mathrm{HC}}(x)F_{\mathrm{HC}}(x)=q\mu_{p,B}p_BF_B \tag{7}$$

holds.

Lee *et al.*[13] reported that the hole mobility of PFB decreases strongly with increasing baking temperature after deposition. Based on their published data the hole mobility of the HC layer, which was baked at 200 °C, can be estimated to be significantly lower than 1×10^{-4} cm^2/V s at low applied electric fields ($<3\times10^4$ V/cm). In contrast for P3HT significantly higher hole mobilities are reported.[16,18] Therefore for low electric fields and for low applied bias voltage, respectively, the hole mobility in the HC, $\mu_{p,\mathrm{HC}}$ can be assumed to be much lower than the one in the blend, $\mu_{p,B}$. This implies that either the hole density or the field (or both of them) has to be much higher in the HC. Changes of the fields are necessarily associated with charges, according to Poisson's equation. A careful analysis should be based on the theory of space charge limited currents yielding spatially varying fields $F_{\mathrm{HC}}(x)$ and hole densities $p_{\mathrm{HC}}(x)$ in the HC. For simplification in the following we will consider constant averages $\langle F_{\mathrm{HC}}\rangle$ and $\langle p_{\mathrm{HCL}}\rangle$. This yields, according to Eq. (7),

$$\frac{\langle p_{\mathrm{HC}}\rangle\langle F_{\mathrm{HC}}\rangle}{p_BF_B}=\frac{\mu_{p,B}}{\mu_{p,\mathrm{HC}}}, \tag{8}$$

where $\langle F_{\mathrm{HC}}\rangle$ and F_B are (roughly) related to each other by Poisson's equation, which reads

$$\langle F_{\mathrm{HC}}\rangle-F_B=\frac{q}{\varepsilon_0\varepsilon_{\mathrm{HC}}}\langle p_{\mathrm{HC}}\rangle d_{\mathrm{HC}} \tag{9}$$

or

$$\langle F_{\mathrm{HC}}\rangle=F_B+\frac{q}{\varepsilon_0\varepsilon_{\mathrm{HC}}}\langle p_{\mathrm{HC}}\rangle d_{\mathrm{HC}} \tag{10}$$

if we assume $\varepsilon_{\mathrm{HC}}\approx\varepsilon_B$ ($\varepsilon_{\mathrm{HC}}$ and ε_B stand for the relative dielectric constants of the HC and the blend and ε_0 for the vacuum permittivity.)

Using Eqs. (3), (8), and (10) the average space charge density in the HC, $\langle p_{\mathrm{HC}} \rangle$, can be expressed by F_B, F_{HC}, and p_B, which yields

$$F_{\mathrm{HC}} = F_B \left(\frac{1}{2} + \sqrt{\frac{1}{4} + \frac{q p_{\mathrm{sat}} d_{\mathrm{HC}}}{\varepsilon_0 \varepsilon F_{\mathrm{sat}}} \frac{\mu_B}{\mu_{\mathrm{HC}}}} \right), \tag{11}$$

with p_{sat} given by Eq. (6).

We now test our predictions on our experiments. From our experiments on the detectors without HC we know the dependence between current density j_B and applied voltage $V_B = F_B d_B$ for the chosen optical power density I_{opt} (dashed line in Fig. 8). This dependence reflects the whole regime from *Schubweg* $\ll d_B$ to *Schubweg* $> d_B$. Equal photocurrents at the same optical power density imply that in addition to the corresponding voltage drop $\Delta V_B(j)$ there is an another voltage drop $\Delta V_{\mathrm{HC}}(j)$ in the HC, which adds up to the total voltage drop V according to Eq. (11) (see full line in Fig. 8). The observed dependence can be understood qualitatively quite well. At low values of $-(V - V_{\mathrm{bi}})$ the field reduction in the blend, according to Eq. (11), is so high that $F_B \ll F_{\mathrm{sat}}$. Hence, the *Schubweg* $\mu_p \tau_p F_B$ is also much shorter than d_B and, accordingly, the photocurrent in the detector $\ll j_{\mathrm{sat}}$. Only if $-(V - V_{\mathrm{bi}})$ exceeds a critical value the charge accumulated in the HC is no longer strong enough to screen the applied voltage efficiently and a further increase of the voltage results in a significant increase of the current.

Equation (11) can describe the distribution of the voltage drops over the two layers ΔV_{HC} and ΔV_B considering that the mobilities of both materials, μ_B and μ_{HC}, are not constant. For disordered materials an electric field dependence of the mobility can be expressed as[19] $\mu = \mu_0 \exp(\gamma \sqrt{F})$. From the plots of the hole mobility versus electric field for P3HT in literature[16,18] γ_B can be estimated to be close to zero as the mobility shows no or only a slight dependence on the electric field. In contrast to that the hole mobility of PFB increases significantly with increasing electric field,[13] thus $\gamma_{\mathrm{HC}} > \gamma_B$. This can explain that $\mu_B / \mu_{\mathrm{HC}}$ becomes lower with increasing values of $-(V - V_{\mathrm{bi}})$. This results in a decrease of F_{HC}/F_B with increasing electric field which is in agreement with the decrease of $\Delta V_{\mathrm{HC}}/\Delta V_B$ with increasing reverse bias voltage, as can be seen in Fig. 8.

After studying the steady state situation the transient response is now discussed (Fig. 9). First the case that the steady state current is extensively reduced by recombination will be focused. When the illumination starts no charge is accumulated and therefore the field within the blend is not lowered [Fig. 7(a), $\mu_p \tau_p F_B > d_B$]. The current density increases to a peak value (Fig. 9, phase A) before the current decreases (Fig. 9, phase B) due to enhanced recombination and finally a steady state value is reached (Fig. 9, phase C). The origin of the recombination is the decreased electric field within the blend caused by charge accumulation [Fig. 7(b); $\mu_p \tau_p F_B < d_B$].

This model is in agreement with the observation that the peak current densities are almost linear with the illumination intensity (Fig. 4) because at the beginning of the illumination

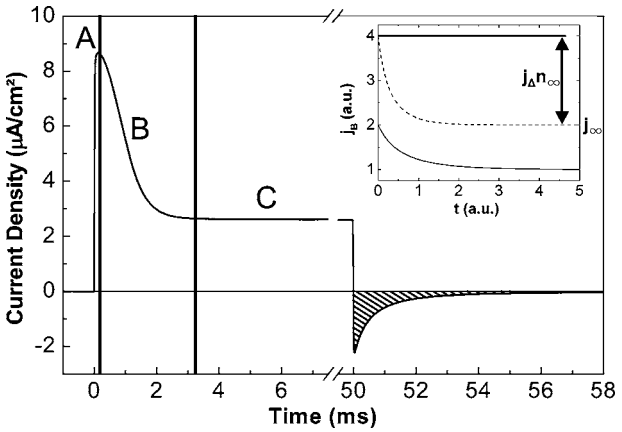

FIG. 9. The different phases of the current transient. No bias voltage is applied to the device and the illumination intensity is 70 μW/cm^2. The inset shows plots of Eq. (18) (see below). As a reference all values of Eq. (18) are set to 1 (solid curve). Doubling j_∞ results in an increased peak value and a shorter transient (dashed curve).

the electric field is not reduced due to charge accumulation and the resulting current is proportional to the photogenerated charge carriers.

It should be mentioned that the rise time of the very initial current increase within phase A is orders of magnitudes faster than the subsequent transient observation caused by charge accumulation [Fig. 6(a)]. Within some microseconds the current increases to 90% of the maximum. This is in agreement with the transit time $t_{\mathrm{tr}} = d^2/\mu V$ of about 2 μs assuming a mobility μ_p 3×10^{-4} cm^2/V s for this material,[16] a thickness d_B of 250 nm, and voltage drop V of 1 V. Also the fact that the rise time becomes shorter with higher reverse bias voltage is an indication that this rise time is dominated by the transit time. For higher reverse bias voltages the determination of the rise time is limited by the experimental setup as mentioned before.

Assuming that all the integrated charge of the negative switch-off current (hatched area in Fig. 9) was accumulated charge at the P3HT-HC interface before, the decrease of the potential drop across the P3HT:PCBM blend $\Delta V_{B,\mathrm{decrease}}$ can be estimated as

$$\Delta V_{B,\mathrm{decrease}} = \frac{Q_{\mathrm{ac}}}{C_B + C_{\mathrm{HC}}} = \frac{Q_{\mathrm{ac}} d_B d_{\mathrm{HC}}}{\varepsilon \varepsilon_0 A (d_b + d_{\mathrm{HC}})}. \tag{12}$$

The integral of the hatched area in Fig. 9 results in a charge density of $Q_{\mathrm{ac}}/A = 2.1 \times 10^{-9}$ C/cm^2. Together with a dielectric constant of $\varepsilon = 3$ for both layer materials as a typical value of a polymer and a layer thickness of $d_B = 250$ nm and $d_{\mathrm{HC}} = 40$ nm the voltage drop $\Delta V_{B,\mathrm{decrease}}$ is about 0.27 V. In the *I-V* characteristics of the photocurrent I_{ph} the voltage offset ΔV_{HC} between the curves of the devices with and without HC is about 0.3 V (Fig. 8). This is close to the calculated value for $\Delta V_{B,\mathrm{decrease}}$, indicating that the negative switch-off current has its origin in the decay of the accumulated charge.

By applying a sufficiently high reverse bias voltage the voltage drop due to accumulation is too low to fulfill the constraint $\mu_p \tau_p F_B < d_B$ for the steady state situation, as depicted in Fig. 9 (for a bias voltage of −1 V). As a consequence the steady state current density is not lowered in

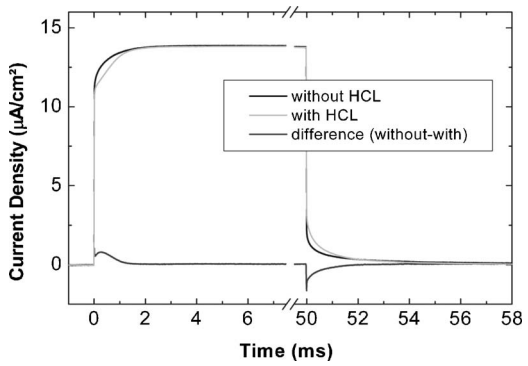

FIG. 10. Current transients for a device with and without HC and the difference of the curves which shows the occurrence of charge accumulation for the device without HC. The applied bias voltage is −1 V and the illumination intensity is 70 μW/cm^2.

comparison with a device without HC, as shown in Fig. 10. Charge accumulation can still be observed by a slightly decreased (increased) current in the switch-on (switch-off) transient. This effect appears even more obvious in the difference of the current densities of a device with HC and without. By applying an even higher reverse bias voltage (−2 V or more), no such transients can be observed in the difference of the currents. Therefore the accumulation probability seems to be dependent on the electric field.

In the following an analytical model for the case $\mu_p \tau_p F_B < d_B$ (recombination regime) is presented which is able to explain the observations qualitatively. This model is based on the assumption that a buildup of charge at the blend/HC interface is due to trapping of holes. The rate of carrier capture can be written as

$$\dot{n}_t = (n_\infty - n_t) c j_B, \tag{13}$$

where c is the trapping probability, n_∞ is the number of occupied traps at steady state situation, and j_B is the current through the blend:

$$j_B = j_s \frac{\tau_p}{t_{\mathrm{tr},B}} = j_s \frac{\tau_p \mu_p F_B}{d_B} = j_s \frac{\tau_p \mu_p}{d_B^2} \left(V_0 - V_{\mathrm{HC},i} - \frac{q n_t}{C_{\mathrm{HC}} + C_B} \right). \tag{14}$$

Here j_s is the saturation current density, τ_p is the recombination lifetime for holes, μ_p is the hole mobility of the P3HT:PCBM blend which can be assumed to be equal to the hole mobility of P3HT, q is the elementary charge, V_0 is the voltage drop over the whole sample, which is determined by the applied voltage and the built-in voltage, $V_{\mathrm{HC},i}$ is the voltage drop over the HC before illumination, and C_{HC} and C_B are the capacitances of the layers. Equations (1) and (2) result in

$$\dot{n}_t - c j_g (n_\infty - n_t)^2 - c j_\infty (n_\infty - n_t) = 0, \tag{15}$$

with

$$j_\infty = j_s \frac{\tau_p \mu_p}{d_B^2} \left(V_0 - V_{\mathrm{HC},i} - \frac{q n_\infty}{C_{\mathrm{HC}} + C_B} \right), \tag{16}$$

$$j_\Delta = j_s \frac{\tau_p \mu_p q}{d_B^2 (C_{\mathrm{HC}} + C_B)}. \tag{17}$$

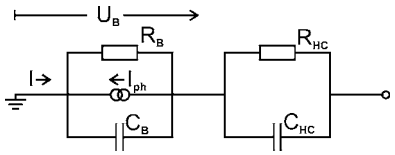

FIG. 11. Equivalent circuit diagram of the system blend layer/HC layer.

The solution of the differential equation (3) results in the following equation for the current j_B:

$$j_B = j_\infty \frac{\left(1 + \frac{j_\infty}{j_\Delta n_\infty} \right) \exp(c j_\infty t)}{\left(1 + \frac{j_\infty}{j_\Delta n_\infty} \right) \exp(c j_\infty t) - 1}. \tag{18}$$

The term j_∞ can be identified as the steady state current density and the product $j_\Delta n_\infty$ is equal to the decrease of the current transient $j_B(t=0) - j_\infty$. The inverse of the factor $c j_\infty$ in the exponent can be interpreted as the time constant of the transient. This model explains the experimental observations in a plausible way. By increasing the illumination intensity the current peak becomes more pronounced and the transients become shorter (Fig. 4). Equation (18) reproduces this observation: Increasing the light intensity results in an increased saturation current j_s which is proportional to j_∞. So the peak values become higher and the transients become shorter (inset of Fig. 9). This is physically clear because more charge carriers are generated and therefore the trap states are occupied faster.

The negative switch-off transient in Fig. 6(a) can be understood by using an equivalent circuit diagram, as displayed in Fig. 11. The blend layer is represented by a resistor R_B, a capacitor C_B, and a current source I_{ph} connected in parallel. The HC is represented by a combination of a resistor R_{HC} and a capacitor C_{HC}.

By application of Kirchhoff's laws to this equivalent circuit the following differential equation can be derived:

$$(C_B + C_{\mathrm{HC}}) \dot{U}_B + (R_B^{-1} + R_{\mathrm{HC}}^{-1}) U_B + I_{\mathrm{ph}} - U_0 R_{\mathrm{HC}}^{-1} = 0. \tag{19}$$

The solution of this equation leads to an expression of the form $I = a + b \exp(-t/c)$ for the current. The analysis of the term b results in the conclusion that the switch-on and switch-off transients of the shape displayed in Fig. 9 (zero bias voltage) appear for the constraint $R_B C_B < R_{\mathrm{HC}} C_{\mathrm{HC}}$. The experiment shows that this negative switch-off current vanishes for higher reverse bias voltages [Fig. 6(a)]. This behavior corresponds to the constraint $R_B C_B > R_{\mathrm{HC}} C_{\mathrm{HC}}$, which indicates that the mobilites μ_B and μ_{HC}, and so R_B and R_{HC}, respectively, depend on the electric field as described before.

V. CONCLUSIONS

In summary it was shown that the dark reverse current of an organic photodiode based on a P3HT:PCBM blend can be reduced by the implementation of an appropriate hole conducting layer. The dynamic response to light excitation was studied by current transient measurements depending on il-

lumination intensity, layer thickness, and bias voltage. A model was presented to explain the shapes of the resulting transients.

By choosing an appropriate bias voltage, the positive effect of dark current reduction can be combined with high external quantum efficiency and good signal linearity of the photodetector. Devices with a response time of less than 2 ms can be realized, which makes them suitable for many applications.

[1]C. W. Tang and S. A. Van Slyke, Appl. Phys. Lett. **51**, 913 (1987).
[2]R. H. Friend *et al.*, Nature (London) **397**, 121 (1991).
[3]D. Dimitrakopoulos and P. R. L. Melenfant, Adv. Mater. (Weinheim, Ger.) **14**, 99 (2002).
[4]G. Yu, J. Gao, J. C. Hummelen, F. Wudl, and A. J. Heeger, Science **270**, 1789 (1995).
[5]N. S. Sariciftci, L. Smilowitz, A. J. Heeger, and F. Wudl, Science **258**, 1474 (1992).
[6]J. J. M. Halls, C. A. Walsh, N. C. Greenham, E. A. Marseglia, R. H. Friend, S. C. Moratti, and A. B. Holmes, Nature (London) **376**, 498 (1995).
[7]J. G. Müller, J. M. Lupton, J. Feldmann, U. Lemmer, M. C. Scharber, N. S. Sariciftci, C. J. Brabec, and U. Scherf, Phys. Rev. B **72**, 195208 (2005).
[8]G. Zerza, C. J. Brabec, G. Cerullo, S. De Silvestri, and N. S. Sariciftci, Synth. Met. **119**, 637 (2001).
[9]N. S. Sariciftci and A. J. Heeger, Int. J. Mod. Phys. B **8**, 237 (1994).
[10]H. Hoppe and N. S. Sariciftci, J. Mater. Res. **19**, 12924 (2004).
[11]P. Schilinsky, C. Waldauf, J. Hauch, and C. J. Brabec, Thin Solid Films **451–452**, 105 (2004).
[12]S. M. Sze, *Physics of Semiconductor Devices* (Wiley, New York, 1981), Chap. 13.
[13]T.-W. Lee, M.-G. Kim, S. Y. Kim, S. H. Park, O. Kwon, T. Noh, and T.-S. Oh, Appl. Phys. Lett. **89**, 123505 (2006).
[14]H. B. Michaelson, J. Appl. Phys. **48**, 4729 (1977).
[15]P. Schilinsky, C. Waldauf, and C. J. Brabec, Appl. Phys. Lett. **81**, 3885 (2002).
[16]S. A. Choulis, Y. Kim, J. Nelson, D. D. C. Bradley, M. Giles, M. Shkunov, and I. McCulloch, Appl. Phys. Lett. **85**, 3890 (2004).
[17]M. Onoda, K. Tada, A. A. Zakhidov, and K. Yoshino, Thin Solid Films **331**, 76 (1998).
[18]S. S. Pandey, W. Takashima, S. Nagamatsu, T. Endo, M. Rikukawa, and K. Kaneto, Jpn. J. Appl. Phys., Part 2 **39**, L94 (2000).
[19]B. Movaghar, M. Grünewald, B. Ries, H. Bässler, and D. Würtz, Phys. Rev. B **33**, 5545 (1986).